Suppression of laser power error in a miniaturized atomic co-magnetometer based on split ratio optimization

Wei-Jia Zhang(张伟佳)[1], Wen-Feng Fan(范文峰)[1,2,†], Shi-Miao Fan(范时秒)[1,2], and Wei Quan(全伟)[2]

[1] *School of Instrumentation Science and Opto-electronics Engineering, Beihang University, Beijing* 100190, *China*
[2] *Beihang Hangzhou Innovation Institute Yuhang, Xixi Octagon City, Yuhang District, Hangzhou* 310023, *China*

(Received 9 June 2022; revised manuscript received 13 July 2022; accepted manuscript online 18 July 2022)

A miniaturized atomic spin-exchange relaxation-free (SERF) co-magnetometer measures angular velocity using a balanced polarimetry technique which is easily affected by the laser power. A laser power closed-loop control system is usually used to suppress the fluctuation of the laser power. Although this method can greatly eliminate the fluctuation of the in-loop laser power (the feedback laser), it cannot fully eliminate the fluctuation of the out-of-loop laser power (the signal measurement laser). This leads to SERF gyroscope laser power error, which reduces the inertial measurement accuracy. In this paper, the influence mechanism of the split ratio (the ratio of the in-loop laser power to the out-of-loop laser power) on the out-of-loop laser power control accuracy is analyzed by establishing a laser power transmission model inside and outside the loop. Moreover, a method is developed to improve the out-of-loop laser power stability by optimizing the split ratio. Comparative experiments showed that the relative Allan standard deviation of the out-of-loop laser power decreased from 5.48×10^{-6} to 2.62×10^{-6} at 100 s, and decreased by an order of magnitude from 1.76×10^{-5} to 3.30×10^{-6} at 1000 s. Correspondingly, the rate ramp coefficient in the Allan standard deviation curve of the SERF gyroscope test data decreased from 1.312 [(°/h)/h] to 0.246 [(°/h)/h]. And the bias stability increased from 0.032 °/h to 0.019 °/h. Therefore, the proposed method can improve the long-term stability of the probe laser power and effectively suppress the laser power error of the SERF gyroscope.

Keywords: atomic gyroscope, spin-exchange relaxation-free, laser power stability, error suppression

PACS: 07.07.Df, 07.55.Ge, 42.79.–e **DOI:** 10.1088/1674-1056/ac81b1

1. Introduction

Co-magnetometers are a series of magnetometers using at least two spin species with different gyromagnetic ratios occupying the same volume.[1–4] The co-magnetometer is widely used in the field of fundamental physics such as searches for electric dipole moments of neutron, violation of local Lorentz invariance, dark matter detection[5–9] due to its ultra-high sensitivity. The co-magnetometer studied in this study is one kind of inertial measurement device that can measure the angular velocity of the carrier with ultra-high sensitivity by means of hybrid atomic spin ensembles working in the spin-exchange relaxation-free regime. The SERF co-magnetometer is considered as a promising compact high-precision gyroscope candidates for long-term navigation systems in the near future.[10–13] Although the performance of an SERF co-magnetometer based on ^{21}Ne is estimated to rival those of traditional gyroscopes, literature has shown that a K–Rb–^{21}Ne SERF co-magnetometer can only achieve a bias instability slightly better than 0.01 °/h.[14,15]

Laser power and frequency stability, magnetic noise amplitude and its drift, and atomic vapor cell temperature stability are some factors that affect the long-term stability of the SERF co-magnetometer.[15–18] The balanced polarimetry technique in the SERF co-magnetometer realizes the angular velocity measurement by measuring the change of the probe laser power. As a result, the fluctuation of the probe laser power is directly coupled to the output signal. Therefore, the stability of probe laser power and the suppression of laser power error is particularly important for improving the long-term performance of the SERF co-magnetometer.[19]

A typical external modulation laser power stabilization system (LPSS) consists of a feedback control circuit and an actuator.[20] The feedback control circuit can use a proportional-integral-derivative (PID) controller, and the actuator can use active devices, such as liquid crystal variable phase retarder (LCVR), electro–optic modulator (EOM), and acousto–optic modulator (AOM). The LPSS usually uses a negative feedback loop, *i.e.*, a part of the main beam is separated by a beam splitter (BS) and detected by a photodetector (PD). The error signal is obtained by difference between the set value and feedback value. The optical loss or gain of the actuator can be changed based on the error signal to stabilize the laser power. However, this method can only effectively control the in-loop laser power, leaving the out-of-loop laser power with significant fluctuations and drifts.[21,22]

As the stability of the out-of-loop laser power is much worse than that of the in-loop one, a few papers have reported specific analyses and solutions. The authors in Ref. [23] showed differences between the stability of the in-loop laser power and the out-of-loop laser power as early as 2006, which

†Corresponding author. E-mail: fanwenfeng@buaa.edu.cn

© 2023 Chinese Physical Society and IOP Publishing Ltd

have not been resolved. The authors in Ref. [24] experimentally verified that the performance of the PD restricts the improvement of laser power stability in the gravitational wave detection frequency band. The authors in Ref. [25] found that the feedback signal delay caused by the slow response speed of the AOM can reduce the stability of the laser power. This paper found that the stability factor reaches its peak by optimizing the operating point of the AOM. However, this method is only applicable to AOM system, which is not conducive to the miniaturization of SERF co-magnetometer. Paris Observatory's research team (2018) assessed the in-loop and out-of-loop laser power stability of the AOM laser power stabilization technology and found that the fluctuation of the out-of-loop laser power may be due to the influence of ambient temperature on the actuators, PBS and PD. The PBS was replaced by a polarization and temperature insensitive uncoated glass plate to pick up the laser beam.[21] However, the SERF co-magnetometer uses the linear polarization of the laser to measure the signal. The uncoated glass plate may introduce polarization errors and reduce the detection accuracy of the SERF co-magnetometer. Therefore, it is necessary to study new technologies to improve the out-of-loop laser power stability.

This study first establishes the in-loop and out-of-loop laser power transmission models of the external modulation LPSS, which reveal that the main factor causing the out-of-loop laser power drift is the fluctuation of the split ratio of the polarization beam splitter (PBS). The split ratio is then theoretically analyzed and optimized to make the system work where it is least sensitive to external disturbances. It is experimentally verified that the laser power error of SERF co-magnetometer and the rate ramp coefficient can be suppressed based on split ratio optimization. As the implement of this method requires no additional optics, it is also beneficial for the miniaturization SERF co-magnetometer.

2. Principle and method

2.1. Signal detection principle of SERF co-magnetometer

The time evolution of the coupled atomic spin ensembles in the SERF co-magnetometer can be described using a set of Bloch equations as follows:[7]

$$\frac{\partial \boldsymbol{P}^{\mathrm{e}}}{\partial t} = \frac{\gamma^{\mathrm{e}}}{Q\left(P^{\mathrm{e}}\right)}\left(\boldsymbol{B}+\lambda M^{\mathrm{n}}\boldsymbol{P}^{\mathrm{n}}+\boldsymbol{L}\right)\times\boldsymbol{P}^{\mathrm{e}}+\boldsymbol{\Omega}\times\boldsymbol{P}^{\mathrm{e}} + \frac{R_{\mathrm{p}}\boldsymbol{s}_{\mathrm{p}}+R_{\mathrm{se}}^{\mathrm{en}}\boldsymbol{P}^{\mathrm{n}}+R_{\mathrm{m}}\boldsymbol{s}_{\mathrm{m}}-R_{\mathrm{tot}}^{\mathrm{e}}\boldsymbol{P}^{\mathrm{e}}}{Q\left(P^{\mathrm{e}}\right)}, \tag{1}$$

$$\frac{\partial \boldsymbol{P}^{\mathrm{n}}}{\partial t} = \gamma^{\mathrm{n}}\left(\boldsymbol{B}+\lambda M^{\mathrm{e}}\boldsymbol{P}^{\mathrm{e}}\right)\times\boldsymbol{P}^{\mathrm{n}}+\boldsymbol{\Omega}\times\boldsymbol{P}^{\mathrm{n}} + R_{\mathrm{se}}^{\mathrm{ne}}\left(\boldsymbol{P}^{\mathrm{e}}-\boldsymbol{P}^{\mathrm{n}}\right)-R_{\mathrm{tot}}^{\mathrm{n}}\boldsymbol{P}^{\mathrm{n}}, \tag{2}$$

where $\boldsymbol{P}^{\mathrm{e}}$ and $\boldsymbol{P}^{\mathrm{n}}$ represent the polarization vectors of electron spin and nuclear spin, respectively; γ^{e} and γ^{n} represent the gyromagnetic ratios of electron and ^{21}Ne, respectively; $\lambda M^{\mathrm{e}}\boldsymbol{P}^{\mathrm{e}}$ and $\lambda M^{\mathrm{n}}\boldsymbol{P}^{\mathrm{n}}$ represent the magnetic fields generated by the spin of alkali atoms and noble gas atoms, respectively; Q is the slowing down factor, $\boldsymbol{B}$ is the ambient magnetic field, $\boldsymbol{L}$ is the light shift, $\boldsymbol{\Omega}$ represents the rotation, R_{p} and R_{m} represent the pumping rates of the pump laser and the probe laser, respectively; $\boldsymbol{s}_{\mathrm{p}}$ and $\boldsymbol{s}_{\mathrm{m}}$ represent the optical pumping vectors of the pump laser and the probe laser, respectively (for circularly polarized light, $\boldsymbol{s}=1$, and for linearly polarized light, $\boldsymbol{s}=0$); $R_{\mathrm{se}}^{\mathrm{en}}$ and $R_{\mathrm{se}}^{\mathrm{ne}}$ represent the spin-exchange rates between the electron spin and nuclear spin, respectively; $R_{\mathrm{tot}}^{\mathrm{e}}$ and $R_{\mathrm{tot}}^{\mathrm{n}}$ represent the total relaxation rates of the electron spin and nuclear spin, respectively.

When the system works at the so-called compensation point, the steady-state solution of Eq. (1) can be solved by setting the left side to zero. The projection of electron spin polarization on the probe direction (assuming that the pump direction is along the z axis and the probe direction is along the x axis) can then be expressed as

$$P_x^{\mathrm{e}} \approx \frac{P_z^{\mathrm{e}}\gamma^{\mathrm{e}}}{R_{\mathrm{tot}}^{\mathrm{e}}}\frac{\Omega_y}{\gamma^{\mathrm{n}}}. \tag{3}$$

The polarized cell works as an optical circular birefringent medium and the atomic spin precession can be detected by measuring the optical rotation of linearly polarized probe laser transmitting the cell. The optical rotation θ can be expressed as

$$\theta = \frac{1}{2}lcr_{\mathrm{e}}f_{\mathrm{D1}}nP_x^{\mathrm{e}}\frac{\nu_{\mathrm{pr}}-\nu_{\mathrm{D1}}}{\left(\nu_{\mathrm{pr}}-\nu_{\mathrm{D1}}\right)^2+\left(\Gamma_{\mathrm{D1}}/2\right)^2}, \tag{4}$$

where l, c, r_{e}, f_{D1}, n, ν_{pr}, ν_{D1}, and Γ_{D1} represent the path length of light passing through the atomic vapor cell, speed of light in vacuum, classical electron radius, oscillation factor, density of Rb, operating frequency of the probe light, resonant frequency of line D1 of Rb, and pressure broadening, respectively.

The balanced polarimetry technique is used for optical rotation detection in our SERF co-magnetometer and the principle diagram is shown in Fig. 1. The light emitting from the laser diode is transformed into linearly polarized light after transmitting the linear polarizer (LP). The polarization plane of the linearly polarized light rotates an angle after passing through the atomic vapor cell due to the circular birefringence. The PBS, PD1, and PD2 constitute a balanced polarimeter whose output is proportional to the optical rotation angle. The angle between the optical axis of the PBS and LP is 45°.

The signals detected by PD1 and PD2 can be calculated as

$$I_1 = I_0\sin^2\left(\theta-\frac{\pi}{4}\right), \tag{5}$$

$$I_2 = I_0\cos^2\left(\theta-\frac{\pi}{4}\right), \tag{6}$$

where I_0 is the laser power incident on the atomic cell. The difference between the two signals can be calculated as $I_1 - I_2 = I_0 \sin 2\theta \approx 2I_0\theta \propto I_0$. It can be seen that the output signal has a first-order correlation with I_0. Obviously, the variation of the I_0 can cause the laser power error, thus reducing the measurement accuracy of the SERF co-magnetometer.

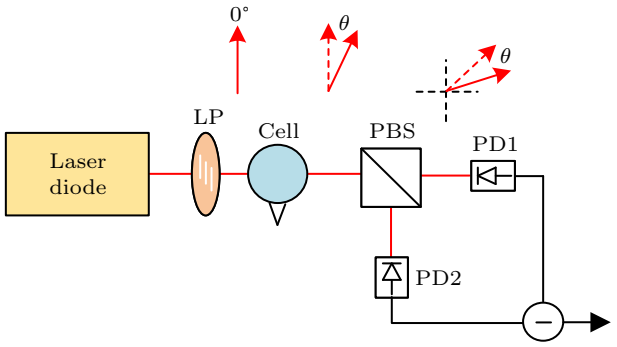


Fig. 1. Schematic diagram of the balanced polarimetry technique. LP: linear polarizer, PBS: polarization beam splitter, PD1 and PD2: photodetectors.

2.2. Laser power transmission model

As is shown in Fig. 2, a bare LCVR (Meadowlark Optics, LVR-065) is used as the actuator in the LPSS of the SERF co-magnetometer. The balanced polarimetry technique is then used to detect the atomic spin precession signal. An LCVR and two polarizers whose optical axes are perpendicular to each other forms an optical power attenuator. It should be emphasised that a Glan–Taylor prism (GT) with a high extinction ratio is selected as the analyzer to prevent the LCVR from introducing polarization errors.[26] The combination of a half wave plate and PBS form a multiplexing structure of beam splitter and polarizer. The split ratio of PBS can be arbitrarily selected by rotating the angle of the optical axis of the half wave plate. The reflected light from the PBS is incident on PD3 (Hamamatsu, S1337-66BR) and is then used as the feedback laser of the LPSS. The transmitted light from the PBS (the stable out-of-loop laser) is incident on the cell to detect the atomic spin precession signal. Finally, the balanced polarimeter which is composed of a Wollaston prism (WP) and two photodetectors (PD1 and PD2) outputs the inertial measurement signal.

Firstly, a transmission model for the probe laser power fluctuation is established. P_0 represents the laser power emitted by the laser source. R and T represent the reflection coefficient and transmission coefficient of the beam splitter composed of half wave plate and PBS, respectively, and $R+T=1$. G_p, V_ref, K_V, and η represent photoelectric conversion coefficient of PD3, reference voltage, control voltage output by PID controller, and voltage-optical power conversion coefficient of optical power attenuator, respectively.

Based on the working principle of the optical power attenuator, the relationship between the laser power after GT (P) and the laser power emitted by the laser source P_0 can be expressed as

$$P_0 - P = (PRG_\mathrm{P} - V_\mathrm{ref})K_\mathrm{V}\eta, \tag{7}$$

where P can be expressed as

$$P = \frac{P_0 + V_\mathrm{ref}K_\mathrm{V}\eta}{1 + K_\mathrm{V}\eta RG_\mathrm{P}}. \tag{8}$$

And the in-loop laser power can be expressed as

$$P_\mathrm{R} = PR = \frac{P_0R + V_\mathrm{ref}K_\mathrm{V}\eta R}{1 + K_\mathrm{V}\eta RG_\mathrm{P}}. \tag{9}$$

When the control parameter of the electronic control system satisfies the condition that $K_\mathrm{V}\eta \to \infty$, the fluctuation of P_0 can be effectively suppressed. We can get $P_\mathrm{R} \to V_\mathrm{ref}/G_\mathrm{P}$, which represents that the output of PD3 is firmly locked to the reference voltage at this time, thus stabilizing the in-loop laser power.

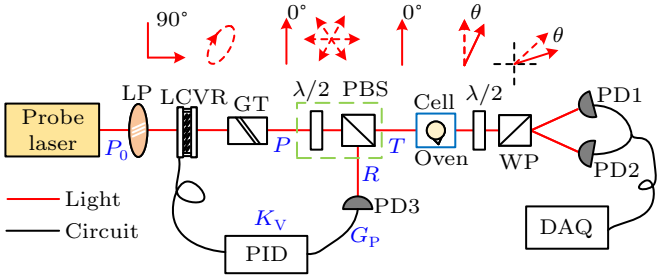


Fig. 2. Schematic diagram of the probe system of the SERF co-magnetometer with an LPSS. LP: linear polarizer, LCVR: liquid crystal variable phase retarder, GT: Glan–Taylor prism, λ/2: half wave plate, PBS: polarization beam splitter, WP: Wollaston prism, PD: photodetector, DAQ: data acquisition board.

For the out-of-loop laser power P_T, it can be expressed as

$$P_T = PT = \frac{P_0T + V_\mathrm{ref}K_\mathrm{V}\eta T}{1 + K_\mathrm{V}\eta RG_\mathrm{P}}. \tag{10}$$

Similarly, when the control parameter of the electronic control system satisfies the condition that $K_\mathrm{V}\eta \to \infty$, we can get $P_T \to TV_\mathrm{ref}/RG_\mathrm{P}$. It can be seen that P_T is related to both the reference voltage and the split ratio of the PBS, where $\mathrm{SR} = R/T$. It is obvious that the feedback control system can only effectively suppress the drift of the laser source, but it can do nothing to suppress the fluctuation of the out-of-loop laser power induced by the variation of split ratio.

In this study, the relative fluctuation of P_T is quantitatively evaluated with differential calculation of the out-of-loop laser power expression as follows:

$$\frac{\mathrm{d}(P_T)}{P_T} \approx -\frac{\mathrm{d}R}{RT}. \tag{11}$$

According to Eq. (11), the relative fluctuation of the out-of-loop laser power is proportional to the fluctuation of the reflection coefficient of the PBS and the scale factor is $1/RT$. Therefore, this scale factor can be minimized by optimizing the split ratio operating point. In this way, the influence of the fluctuation of the split ratio on the out-of-loop laser power can be reduced, which is beneficial to improve the laser power stability.

3. Experimental setup

The experimental test of the influence of the split ratio fluctuation on the out-of-loop laser power is carried out to verify the described model and theoretical predictions. The schematic diagram of the experimental setup is shown in Fig. 3. The whole system has four main components, namely, atomic vapor cell, magnetic shielding system, pumping system, and probing system. As the core-sensitive component, the atomic vapor cell is a spherical cell made of aluminosilicate glass with an outer diameter of 10 mm. The cell contains a small drop of alkali metal potassium (K) and rubidium (Rb) mixture, 1 atm (1 atm = 1.01325×10^5 Pa) of neon (^{21}Ne), and 50 Torr (1 Torr = 1.33322×10^2 Pa) of nitrogen (N_2). The cell is fixed in a boron–nitride oven, and its temperature is stabilized at 185 °C with a non-magnetic high-frequency AC current heating coil and a PID controller. The atomic number density ratio of K to Rb at this temperature is about 1:160. The entire atomic vapor cell system with heating coils is placed in a magnetic shielding system composed of three layers of permalloy and an inner layer of manganese–zinc (Mn–Zn) ferrite to eliminate environmental magnetic field fluctuations. Moreover, a set of three-axis magnetic field compensation coil is installed inside the magnetic shielding cylinder to further eliminate the residual magnetic field and ensure that the electron spin is in the SERF regime. For the pumping system, a small fraction of the pump laser is separated to stabilize the pump laser frequency at the D1 line of K using the saturated absorption technology after the pump laser with a frequency of 770.108 nm is emitted from the distributed Bragg reflection (DBR) laser diode. An LCVR is used to stabilize the laser power at 30 mW. Additionally, the diameter of the pumping spot is enlarged to 6 mm through the lens. Finally, a quarter wave plate is used to turn the pump laser into circularly polarized light. The circularly polarized light enters the atomic vapor cell to polarize the atomic spin along the z axis. For the probing system, the other LCVR is used to stabilize the probe laser power at 1 mW after the probe laser with a frequency of about 795.115 nm is emitted from a distributed feedback (DFB) laser diode. The combination of a half wave plate and PBS1 is used for laser beam splitting and as a polarizer. The reflected light passing through PBS1 is used as the in-loop light for laser power stabilization. The linearly polarized transmitted light then enters the cell for signal detection. Notably, the half wave plate and PBS1 are placed after the mirror to avoid the polarization error introduced by the mirror. The WP, PD3, and PD4 constitute the polarization balanced polarimeter, which is used to measure the spin polarization of atoms along the x axis. Finally, the data acquisition board (DAQ, NI USB-4431) is used to record the data. In the probing system, any split ratio of the PBS1 is achievable by rotating the optical axis angle of the half wave plate in front of PBS1. In order to evaluate the stability of the laser power before and after the optimization of the split ratio, an additional PD5 can be installed at the position shown in the blue dashed box in the Fig. 3, and the data is detected by a power meter. Then, in order to evaluate the suppression effect of the optimized split ratio on the laser power error of the SERF co-magnetometer, PD5 was removed, and the inertial signal at different split ratios was measured using the balanced polarimeter behind the atomic vapor cell for comparison.

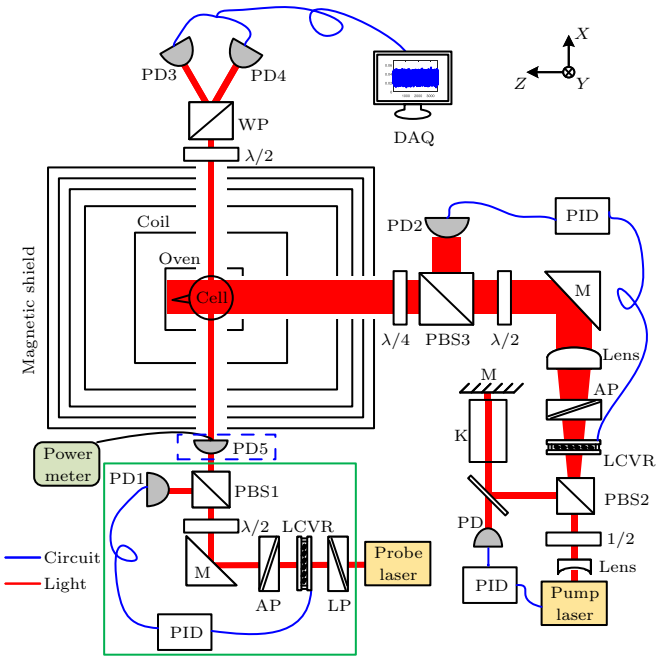


Fig. 3. Schematic diagram of the working principle of SERF co-magnetometer. LP: linear polarizer, AP: analyzer, $\lambda/2$: half wave plate, $\lambda/4$: quarter wave plate, M: reflecting mirror, LCVR: liquid crystal variable phase retarder, GT: Glan–Taylor prism, PBS: polarization beam splitter, WP: Wollaston prism, PD: photodetector. DAQ: data acquisition board.

4. Experimental results and discussion

The laser power stability tests and SERF inertial measurement experiments were conducted under different split ratio conditions using the built SERF co-magnetometer. First, the difference of laser power stability between the in-loop and the out-of-loop in the LPSS was assessed (data recording length = 2 hours). The in-loop laser power was detected by the PD1, while the out-of-loop laser power was detected by a newly added PD. The PD was connected to a self-made trans-impedance photo-current amplifier with an amplification factor of 2000 V/A, converting the photo-current into a voltage signal. Finally, the voltage signal was collected by the DAQ at a sampling frequency of 200 Hz. The time-domain test results of a group of laser power fluctuations are shown in Fig. 4. The value of the vertical coordinate shows that the split ratio at this point is 0.39:0.61. It can be seen from Fig. 4(a) that the in-loop laser power can be firmly fixed at 0.66 V by real-time gain or attenuation of the laser power. The out-of-loop laser power in Fig. 4(b) has significant fluctuations and drifts. These fluctuations and drifts of the out-of-loop laser power greatly affect

the measurement accuracy of the SERF co-magnetometer, introducing laser power error.

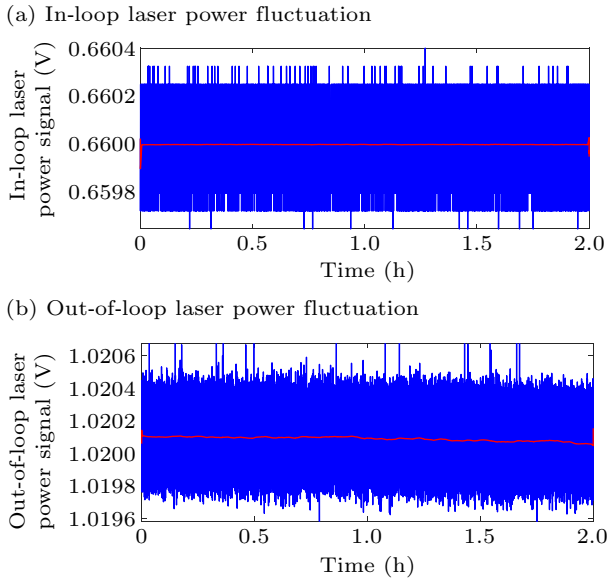


Fig. 4. The laser power fluctuation after closed-loop control: (a) the in-loop laser power, (b) the out-of-loop laser power.

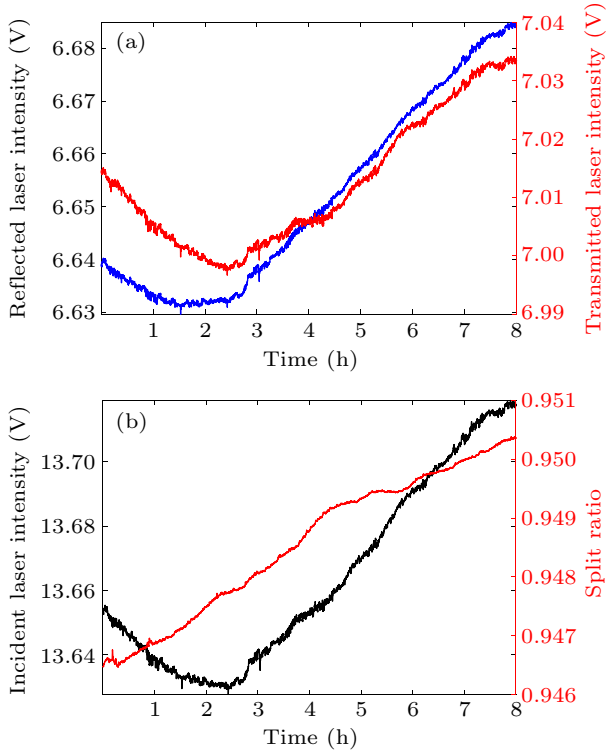


Fig. 5. Drift measurements of the split ratio of PBS with the fluctuation of the laser power. (a) The fluctuations of the reflected laser intensity and the transmitted laser intensity. (b) The fluctuations of the incident laser intensity and the split ratio.

According to the analysis in Section 2, the fluctuation of the reference voltage and the split ratio caused this phenomenon based on the established out-of-loop laser power transmission model. Subsequently, laser power error suppression is conducted based on split ratio optimization. As shown in Fig. 5, the split ratio fluctuation of the PBS in the experimental setup was tested. Obviously, the split ratio is not fixed, but drifts with the variation of the incident laser power. This indicates that the fluctuation of the out-of-loop laser power is mainly caused by the variation of the split ratio.

In order to quantitatively analyze the influence of the split ratio fluctuation on the out-of-loop laser power drift, the split ratio fluctuation coefficient (the change value of the split ratio caused by the change of laser power per milliwatt) was tested. The non-ideal elliptical component in the linearly polarized light can cause the transverse optical pumping effect and the transverse light-shift when the probe laser power in a SERF co-magnetometer is relatively large, thus increasing the atomic relaxation rate and reducing the inertial measurement sensitivity. The photo current converted by the PD is very weak when the probe laser power is relatively low, making the circuit noise reduce the signal-to-noise ratio. Therefore, the probe laser power entering the atomic vapor cell is usually selected to be about 1 mW. The performance test of the PBS split ratio was performed with the input laser power around 1 mW. It can be seen from the test results in Table 1 and Fig. 6 that the split ratio fluctuation coefficient was 0.03516 mW^{-1}.

Table 1. The PBS split ratio *versus* incident laser power.

Incident laser power (mW)	Reflected power (mW)	Transmitted power (mW)	Split ratio R/T
1.21	0.471	0.708	0.665254
1.12	0.406	0.612	0.663399
1.04	0.366	0.554	0.660650
0.95	0.331	0.502	0.659363
0.86	0.311	0.473	0.657505
0.81	0.279	0.426	0.654930
0.74	0.260	0.399	0.651629
0.69	0.239	0.367	0.651226
0.64	0.220	0.340	0.647059
0.60	0.205	0.318	0.644654
0.56	0.189	0.295	0.640678

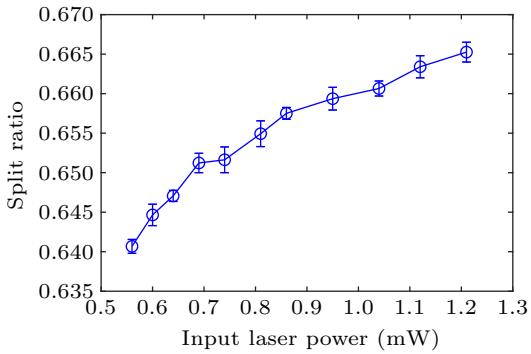


Fig. 6. Variation curve of PBS split ratio with the input laser power.

According to Eq. (11) that the relative fluctuation of the out-of-loop laser power is proportional to the fluctuation of the reflection coefficient of the PBS. Assuming that the input laser power changed by 0.1 mW and the reflection coefficient fluctuation was 0.003516 based on the previous test results of the PBS split ratio, the relative fluctuation of the out-of-loop laser power was numerically simulated and shown

in Fig. 7. Two typical points were selected from the simulation curve for analysis. The reflection coefficients of the two points were 0.10 and 0.50, and the corresponding split ratios were 0.10:0.90 and 0.50:0.50, respectively. The corresponding relative fluctuations of the laser power were 3.91% and 1.41%, respectively. The stability of the out-of-loop laser power can be increased by about 2.78 times by split ratio optimization. The above analysis shows that the closer the split ratio is to 0.50:0.50, the smaller the out-of-loop laser power fluctuation.

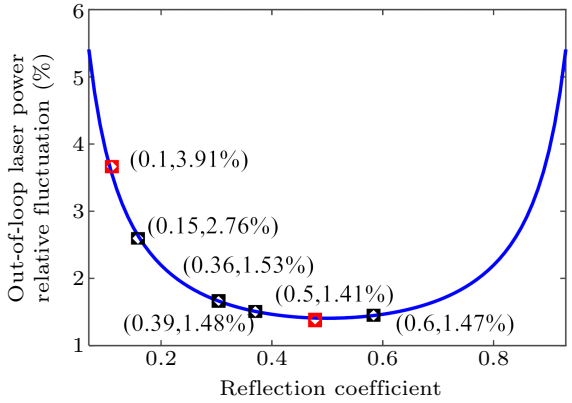


Fig. 7. The relationship between the out-of-loop laser power fluctuation and the reflection coefficient.

The laser power stability of the in-loop and the out-of-loop at different split ratio was tested by rotating the half wave plate in front of PBS1. The time-domain graph of the test result was similar to that in Fig. 4. The relative Allan standard deviation method was adopted to analyze the experimental data (Fig. 8). For the SERF co-magnetometer developed for future long term inertial navigation system, the Allan standard deviation of long cluster time should be the main focus. The in-loop laser power curve of the black line had a downward trend, reaching 2.302×10^{-7} at 100 s. This result could be because the in-loop laser was controlled by a stable closed-loop control, there was no trend item on the Allan standard deviation curve. For the out-of-loop laser power, the red line in the figure corresponded to the relative Allan standard deviation of the out-of-loop laser power with a split ratio of 0.15:0.85. The blue line corresponded to the split ratio of 0.50:0.50. The red and blue lines corresponded to 5.48×10^{-6} and 2.62×10^{-6}, respectively, at the 100-s position, and at 1000-s position, they corresponded to 1.76×10^{-5} and 3.30×10^{-6} . This indicates that the stability is better with a split ratio approaching 0.50:0.50 compared with other curves. The experimental results are consistent with the theoretical simulation results shown in Fig. 7, verifying the correctness of the established out-of-loop laser power transmission model.

To verify that the method proposed in the current study can suppress the laser power error of the SERF co-magnetometer, the bias stability of the SERF co-magnetometer was tested under different split ratios and Allan standard deviation analysis results were shown in Fig. 9. It can be seen that similar to the results in Fig. 8, the stability of the SERF co-magnetometer was better with a split ratio approaching 0.50:0.50 compared with other curves. The value of the red line at the 100-s position was 0.032 °/h, while that of the blue line was 0.019 °/h. Correspondingly, the rate ramp coefficient decreased from 1.312 [(°/h)/h] to 0.246 [(°/h)/h]. This indicates that the time when the trend item dominates has been postponed as the split ratio is close to 0.50:0.50. Therefore, the experimental results verified the effectiveness of the method proposed in the current study.

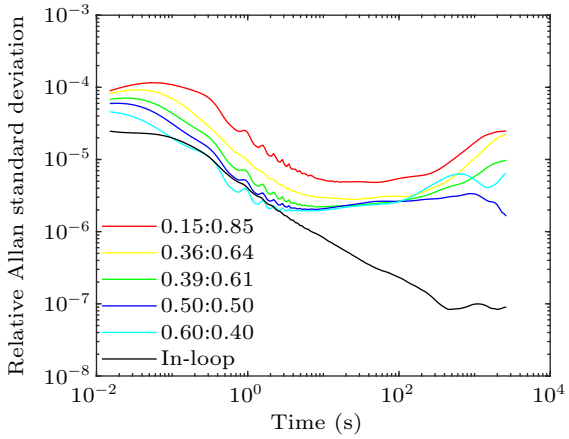


Fig. 8. The relative Allan standard deviation of the laser power fluctuation inside and outside the control loop under different split ratios.

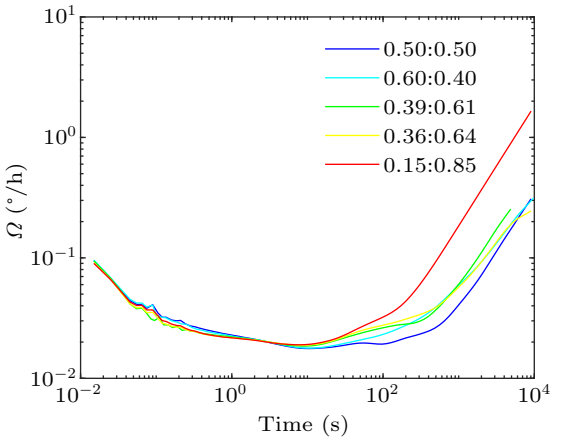


Fig. 9. Allan standard deviation of the SERF co-magnetometer bias stability under different split ratios.

5. Conclusion

In conclusion, the present study has developed a laser power transmission model to to address the problem that the laser power stability inside and outside the control loop in the LPSS is inconsistent. According to the model, the reason for the poor stability of the out-of-loop laser power is mainly due to the fluctuation of the split ratio of PBS. By simulating the quantitative relationship between the fluctuation of the out-of-loop laser power and the fluctuation of the split ratio, a method is proposed to improve the out-of-loop laser power stability by split ratio optimization. Results show that the relative Allan standard deviation of the out-of-loop laser power decreased

from 5.48×10^{-6} to 2.62×10^{-6} at 100 s, and decreased by an order of magnitude from 1.76×10^{-5} to 3.30×10^{-6} at 1000 s. Correspondingly, the rate ramp coefficient in the Allan standard deviation curve of the SERF co-magnetometer test data decreased from 1.312 [(°/h)/h] to 0.246 [(°/h)/h]. The laser power error of SERF co-magnetometer has been effectively suppressed. The model and method proposed in this study provide support for quickly determining the optimal operating point of the LPSS. In the next step, the film material of PBS will be studied to manufacture devices with more stable split ratios, so that the long-term stability of the out-of-loop laser power can be further improved.

Data availability statement

The data that support the findings of this study are openly available in Science Data Bank at the following link https://doi.org/10.57760/sciencedb.j00113.00041

Acknowledgment

Project supported by the National Natural Science Foundation of China (Grant Nos. 61925301 and 62103026).

References

[1] Lamoreaux S K, Jacobs J P, Heckel B R, Raab F J and Fortson E N 1986 *Phys. Rev. Lett.* **57** 3125
[2] Vasilakis G, Brown J, Kornack T and Romalis M 2009 *Phys. Rev. Lett.* **103** 261801
[3] Kimball D F J., Dudley J, Li Y, Patel D and Valdez J 2017 *Phys. Rev. D* **96** 075004
[4] Lee J, Almasi A and Romalis M 2018 *Phys. Rev. Lett.* **120** 161801
[5] Shaham R, Katz O and Firstenberg O 2022 *Nat. Phys.* **18** 506
[6] Jiang M, Su H, Garcon A, Peng X and Budker D 2021 *Nat. Phys.* **17** 1402
[7] Kornack T W 2005 *A test of CPT and Lorentz symmetry using a K-^{3}He co-magnetometer* PhD Dissertation (Princeton University)
[8] Brown J M, Smullin S J, Kornack T W and Romalis M V 2010 *Phys. Rev. Lett.* **105** 151604
[9] Smiciklas M, Brown J, Cheuk L, Smullin S and Romalis M V 2011 *Phys. Rev. Lett.* **107** 171604
[10] Kornack T W, Ghosh R K and Romalis M V 2005 *Phys. Rev. Lett.* **95** 230801
[11] Li R J, Fan W F, Jiang L W, Duan L H, Quan W and Fang J C 2016 *Phys. Rev. A* **94** 032109
[12] Liang Y X, Jiang L W, Liu J L, Fan W F, Zhang W J, Fan S M, Quan W and Fang J C 2022 *Phys. Rev. Appl.* **17** 024004
[13] Jiang L W, Liu J L, Liang Y X, Tian M N and Quan W 2022 *Appl. Phys. Lett.* **120** 074101
[14] Jiang L W, Quan W, Li R J, Fan W F, F. Liu F, Qin J, Wan S A and Fang J C 2018 *Appl. Phys. Lett.* **112** 054103
[15] Fu Y, Fan W F, Ruan J S, Liu Y, Lu Z L and Quan W 2022 *IEEE Trans. Instrument. Meas.* **71** 1
[16] Fan W F, Quan W, Zhang W J, Xing L and Liu G 2019 *IEEE Access* **7** 28574
[17] Liu F, Duan L H, Fan W F, Pang H Y, Liu S X and Quan W 2021 *IEEE Sensors Journal* **22** 1990
[18] Ma D Y, Lu J, Fang X J, Yang K, Wang K, Zhang N, Han B C and Ding M 2022 *IEEE Trans. Industr. Electron.* **69** 991
[19] Fan W F, Quan W, Liu F, Duan L H and Liu G 2019 *Chin. Phys. B* **28** 110701
[20] Xing L, Wang Z, Huang J, Quan W, Fan W F and Jiang L W 2018 13rd *IEEE Conference on Industrial Electronics and Applications (ICIEA)* pp. 735–738
[21] Tricot F, Phung D, Lours M, Guérandel S and Clercq E 2018 *Rev. Sci. Instrum.* **89** 113112
[22] Niu Y, Duan L H, Zhang J X, Huang J, Zhai Y Y and Quan W 2022 *Rev. Sci. Instrum.* **93** 043002
[23] Seifert F, Kwee P, Heurs M, Willke B and Danzmann K 2006 *Opt. Lett.* **31** 2000
[24] Kwee P, Willke B and Danzmann K 2011 *Appl. Phys. B* **102** 515
[25] Balakshy V, Kuznetsov Y I, Mantsevich S and Polikarpova N 2014 *Opt. Laser Technol.* **62** 89
[26] Huang J, Wang Z, Fan W F, Xing L, Zhang W J, Duan L H and Quan W 2020 *Opt. Express* **28** 35748